MatDecompSDF: High-Fidelity 3D Shape and PBR Material Decomposition from Multi-View Images

Chengyu Wang
San Francisco State University
San Francisco, California, USA
dking20@sfsu.edu

Isabella Bennett
Department of Electrical & Computer
Engineering, Boston University
Boston, MA, USA
isabella.bennett@bu.edu

Henry Scott
Department of Electrical & Computer
Engineering, Boston University
Boston, MA, USA
henry.scott@bu.edu

Liang Zhang
University of California, Berkeley
Berkeley, California, USA
lzhang@berkeley.edu

Mei Chen
Stanford University
Stanford, California, USA
meichen@stanford.edu

Hao Li
Carnegie Mellon University
Pittsburgh, Pennsylvania, USA
haoli@cs.cmu.edu

Rui Zhao
University of Washington
Seattle, Washington, USA
ruizhao@uw.edu

Abstract

We present MatDecompSDF, a novel framework for recovering high-fidelity 3D shapes and decomposing their physically-based material properties from multi-view images. The core challenge of inverse rendering lies in the ill-posed disentanglement of geometry, materials, and illumination from 2D observations. Our method addresses this by jointly optimizing three neural components: a neural Signed Distance Function (SDF) to represent complex geometry, a spatially-varying neural field for predicting PBR material parameters (albedo, roughness, metallic), and an MLP-based model for capturing unknown environmental lighting. The key to our approach is a physically-based differentiable rendering layer that connects these 3D properties to the input images, allowing for end-to-end optimization. We introduce a set of carefully designed physical priors and geometric regularizations, including a material smoothness loss and an Eikonal loss, to effectively constrain the problem and achieve robust decomposition. Extensive experiments on both synthetic and real-world datasets (e.g., DTU) demonstrate that MatDecompSDF surpasses state-of-the-art methods in geometric accuracy, material fidelity, and novel view synthesis. Crucially, our method produces editable and relightable assets that can be seamlessly integrated into standard graphics pipelines, validating its practical utility for digital content creation.

Keywords

Inverse Rendering, Physically-Based Rendering (PBR), Neural Implicit Surfaces, 3D Reconstruction, Material Decomposition, Differentiable Rendering

1 Introduction

The demand for high-fidelity, interactive, and editable 3D content has become a cornerstone of modern digital experiences, fueling advancements in virtual and augmented reality, digital twins, and the entertainment industry . Traditionally, creating such photorealistic digital assets is a labor-intensive process, often requiring expert artists to manually model geometry and define complex material properties. The advent of neural scene representations has marked a paradigm shift, offering a new avenue for synthesizing and reconstructing the 3D world directly from images. Groundbreaking work on Neural Radiance Fields (NeRF) demonstrated an unprecedented ability to synthesize photorealistic novel views from a collection of images by representing a scene as a continuous volumetric function [16]. This seminal work spurred a wave of research exploring dynamic scenes [20] and even articulated subjects like humans [13, 28]. However, the implicit volumetric nature of NeRF makes it challenging to extract explicit, high-quality surface geometry, which is crucial for most graphics pipelines.

To address this limitation, a significant body of research has focused on learning neural implicit surface representations, most notably through Signed Distance Functions (SDFs). Frameworks like NeuS [26] and VolSDF [31] ingeniously bridge the gap between volume rendering and surface rendering, enabling the extraction of detailed and coherent meshes from multi-view images. The pursuit of efficiency and detail in these reconstructions continues, with methods exploring explicit representations like tensor decompositions [10, 12] and optimization "baking" strategies to accelerate rendering [5]. This hierarchical refinement of detail, from coarse volumetric fields to precise surfaces, mirrors the effectiveness of hierarchical models in other domains, such as understanding the nested structure of language in sign language translation or parsing complex scenes in visual dialog.

Nevertheless, geometry alone is insufficient for true photorealism. An object's appearance is an intricate interplay of its surface shape, its intrinsic material properties, and the surrounding illumination. The ultimate goal is thus *inverse rendering*: the challenging, ill-posed problem of disentangling these coupled factors from 2D observations. Early explorations in the neural domain sought to factorize NeRF into reflectance and illumination components [3, 41], often under simplified assumptions. Subsequent works have made significant strides by integrating physically-based rendering principles directly into the optimization process. These methods aim to

decompose appearance into standardized Physically-Based Render-ing (PBR) parameters—such as albedo, roughness, and metallic—by leveraging differentiable renderers [35, 37]. This disentanglement is critical, as failing to separate these components can lead to ambigu-ity, a challenge analogous to disambiguating events from correlated signals in audio-visual analysis or grounding language in proposal-free video understanding .

State-of-the-art inverse rendering frameworks have achieved remarkable results, capable of extracting high-quality triangular meshes along with their PBR material maps and complex light-ing environments [18, 39]. These methods have been extended to handle complex indoor scenes [4, 32], unstructured "in-the-wild" online image collections [15], and even animatable human avatars with relightable properties [40]. The development of comprehen-sive frameworks has further unified these disparate efforts. De-spite this progress, significant challenges remain. First, many high-fidelity methods are computationally expensive, hindering their practical application; recent advances in real-time relighting with 3D Gaussians [11] and efficient representations [8] are beginning to address this. The need for efficient models is a universal con-cern, echoing the importance of model compression techniques like multi-objective convex quantization in deploying large networks . Second, most models are limited to simple, opaque materials, strug-gling with optically complex phenomena like translucency [33], anisotropic reflectance [23], or the intricate structure of hair [6]. Third, robustly handling diverse real-world data requires sophisti-cated techniques, from modeling visibility and occlusion [24, 38] to leveraging specialized information like polarization [17].

The recent explosion in large-scale generative models offers a powerful new tool for tackling these challenges. Text-to-2D dif-fusion models have been ingeniously repurposed as powerful 3D priors through score distillation sampling [19], enabling text-to-3D content creation [14]. These generative techniques are evolving to produce higher-fidelity and more diverse results [27] and are increasingly capable of disentangling geometry and appearance in a text-guided manner [7]. This allows for semantic texturing [21] and material assignment [22], where textual concepts like "metallic" or "wooden" are translated into PBR values, a process informed by material-aware image generation [30]. Furthermore, multi-modal models like CLIP facilitate direct, text-driven editing of neural scenes [25], enabling intuitive control over object materi-als [9] and textures [1]. This convergence of vision, language, and graphics points towards a future of highly controllable and seman-tic 3D content creation, akin to how cross-modal understanding enhances tasks like sign language production and crowd counting .

Beyond the visual spectrum, the broader field of sensing is also moving towards extracting nuanced information from ubiquitous signals. The ability to recognize human activities , gestures , emo-tions , and even vital pulmonary functions from commodity WiFi signals showcases a parallel trend of disentangling complex infor-mation from noisy, indirect measurements. The security and privacy implications of such advanced sensing, from fingerprinting attacks to keystroke eavesdropping , highlight a universal need for robust and secure systems, a consideration that will become paramount as 3D reconstruction moves towards distributed, user-sourced data. Architectures for such distributed systems, potentially leveraging

federated learning with neural architecture search and experience-driven model migration , provide a roadmap for future privacy-preserving 3D capture ecosystems. This thesis situates itself within this rich context, aiming to push the boundaries of high-fidelity, physically-based inverse rendering of general objects. We focus on robustly and efficiently disentangling geometry and complex material properties from multi-view images, drawing inspiration from both the explicit structure of physically-based rendering and the powerful priors of modern neural networks [29].

In this thesis, we introduce a novel framework for reconstructing general 3D objects with a focus on accurate, explicit decomposi-tion of their surface materials into physically-based parameters. Our primary contributions are threefold: (1) We propose a new neural representation that effectively disentangles geometry from spatially-varying material properties under unknown illumination. (2) We introduce a set of physics-inspired loss functions and regu-larization techniques that significantly improve the robustness of the decomposition, particularly for non-Lambertian surfaces. (3) We demonstrate through extensive experiments that our recon-structed assets can be seamlessly imported into standard graphics engines for high-fidelity relighting and editing, validating their practical utility. The remainder of this thesis is organized as fol-lows: Chapter 2 reviews related work in detail. Chapter 3 presents our proposed methodology. Chapter 4 describes our experimen-tal setup and results. Finally, Chapter 5 concludes the thesis and discusses promising directions for future work.

2 Related Work

Our work builds upon a rich body of literature spanning neural scene representations, inverse rendering, and generative 3D model-ing. In this section, we review the most relevant prior art in these areas.

2.1 Neural Scene Representations for Geometry

The foundation of modern neural rendering was laid by Neural Ra-diance Fields (NeRF) [16], which represents a scene's geometry and view-dependent appearance using a multilayer perceptron (MLP). While revolutionary for novel view synthesis, NeRF's implicit vol-umetric representation makes extracting a high-quality, explicit surface mesh challenging. To overcome this, a significant line of work has focused on learning neural implicit surfaces, typically parameterized as Signed Distance Functions (SDFs). VolSDF [31] and NeuS [26] were pioneering works in this direction, proposing novel formulations to convert SDFs into volume densities for ren-dering, thereby enabling the optimization of a coherent surface from 2D images. The pursuit of efficiency and quality has led to hybrid representations that combine the benefits of implicit func-tions with explicit data structures, suchas voxel grids or tensor decompositions. For instance, TensoIR [12] and K-Planes [10] uti-lize explicit low-rank tensor representations to achieve significantly faster training and rendering speeds. Other methods focus on "bak-ing" a trained neural field into an explicit structure like a mesh with features, enabling real-time rendering post-optimization [5]. The recent introduction of 3D Gaussian Splatting [8] has offered a pow-erful alternative, representing scenes as a collection of anisotropic Gaussians that can be rendered in real-time with high fidelity. The

challenge of efficiently representing complex data is not unique to 3D vision; similar concerns motivate research in model compression and the design of efficient architectures for tasks ranging from visual dialog to crowd counting .

2.2 Neural Inverse Rendering

Inverse rendering, the process of decomposing a scene into its fundamental components of geometry, material, and lighting, is a classic and notoriously ill-posed problem in computer vision. Neural approaches have made remarkable progress. Early methods extended the NeRF framework to jointly estimate reflectance and illumination. NeRFactor [41] factorized the scene into a shape, a BRDF, and an illumination model represented by spherical harmonics. NeRD [3] further explored reflectance decomposition from challenging in-the-wild images. A crucial step forward was the integration of physically-based differentiable rendering. By incorporating a rendering layer that simulates light transport based on physical principles, models can learn to extract standardized PBR material parameters. PhySG [35] and IRON [37] were influential in demonstrating the joint optimization of neural SDFs with material properties like diffuse albedo and roughness.

The current state-of-the-art is represented by powerful frameworks like NVDIFFREC [18], which directly optimizes a triangle mesh, its PBR materials, and an HDR light map to match input images. Mat-NeuS [34] extends the high-fidelity surface reconstruction of NeuS to simultaneously acquire material properties. Neural-PIL [2] introduced pre-integrated lighting to efficiently handle complex reflectance. These methods have been successfully applied to reconstruct general objects [39] and even full indoor scenes [32]. The core challenge in all these methods is robust disentanglement, which requires careful regularization and priors. This is conceptually similar to the need for robust feature extraction in other domains, such as developing anti-interference techniques for WiFi-based activity recognition or building secure authentication systems resilient to fingerprinting attacks . Our work contributes to this line of research by proposing new techniques to improve the robustness of material decomposition under unknown lighting. We also draw inspiration from how hierarchical models can parse complex structures, a principle proven effective in tasks like sign language translation.

2.3 Generative Priors for 3D Content Creation

The rise of large-scale generative models, particularly 2D diffusion models, has unlocked new paradigms for 3D content creation. DreamFusion [19] introduced Score Distillation Sampling (SDS), a method to "distill" the knowledge of a pre-trained 2D text-to-image model to guide the optimization of a 3D representation like NeRF. This spawned a flurry of research in text-to-3D generation, with follow-up works like Magic3D [14] improving resolution and efficiency. ProlificDreamer [27] proposed Variational Score Distillation (VSD) to enhance the diversity and fidelity of generated results. A key focus of recent work is the disentanglement of geometry and appearance within this generative framework. Fantasia3D [7] and TexFusion [22] explicitly aim to generate not just a shape, but also assign meaningful textures and PBR materials based on textual prompts. This leverages the powerful multi-modal understanding of

joint vision-language models like CLIP. Such models are also used for text-guided editing of existing 3D shapes [21] or neural fields [25], enabling intuitive manipulation of scene properties [9]. The ability to generate content based on abstract, multi-modal inputs resonates with research in visual dialog , video grounding , and even cross-modal emotion recognition , all of which seek to bridge the gap between different data modalities.

2.4 Modeling of Advanced Materials and Dynamic Scenes

While significant progress has been made on opaque, Lambertian surfaces, modeling the full spectrum of real-world materials and dynamics remains an active research frontier. For complex materials, specialized representations are needed. NeRF-V [38] and NeRO [24] explicitly model visibility and occlusion to handle complex shadowing and relighting. Polarized-NeRF [17] leverages polarization cues to better separate diffuse and specular components. For translucent objects with subsurface scattering, methods like Neural Transmitted Radiance Fields [33] model the path of light through the object's interior. Other works tackle anisotropic materials [23] or highly complex microstructures like hair [6]. The challenge of representing complex appearance is also addressed by works that learn decoupled neural textures [1] or extract neural BRDFs [29].

Modeling dynamic and deformable objects presents another set of challenges. D-NeRF [20] pioneered the use of a deformation field to map a dynamic scene to a canonical space. This concept has been extended to create controllable and animatable avatars of human actors , often incorporating relighting capabilities [40]. The ability to track and model human motion finds parallels in other sensing modalities, such as gesture recognition using WiFi . The overarching goal is to build robust models from diverse, often unstructured data, whether it's from online image collections [15] or from distributed agents in a federated learning setting . The security and privacy of such data are paramount, a concern highlighted by research into the vulnerabilities of sensing systems . Our work focuses on static objects but aims for a material representation robust enough to serve as a foundation for future extensions into these more complex dynamic and material domains, where understanding subtle signals, much like in audio-visual event analysis or respiratory healthcare sensing , is key.

3 Methodology

In this section, we present the technical details of our proposed framework, which we name **MatDecompSDF**, for recovering high-fidelity 3D shapes and decomposing their physically-based material properties from multi-view images. Our core idea is to jointly optimize a neural representation for geometry, spatially-varying materials, and scene illumination by leveraging a differentiable renderer that simulates physically-based light transport. The entire framework is trained end-to-end, guided by a set of carefully designed loss functions and physical priors.

3.1 Framework Overview

As illustrated in Figure 1, our framework takes a set of multi-view images of an object, along with their corresponding camera poses

and foreground masks, as input. The output consists of a high-quality explicit surface mesh, and a set of PBR material maps (albedo, roughness, and metallic) that are aligned with the mesh geometry. Our system is composed of three main neural components: 1) a geometry network that represents the shape as a Signed Distance Function (SDF), 2) a material network that predicts spatially-varying PBR parameters on the surface, and 3) a lighting network that models the scene's illumination. During training, we cast rays from the camera, sample points along these rays, and use a differentiable volume renderer to compute the color of each pixel. The discrepancy between the rendered colors and the input images drives the joint optimization of all three network components. This end-to-end optimization is analogous to complex inference processes seen in other domains, such as iterative context-aware graph inference for visual dialog .

3.2 Neural Scene Representation

We represent the scene using three distinct MLPs to effectively disentangle geometry, material, and lighting, a strategy proven more robust than using a single monolithic network [35].

3.2.1 Geometry as a Neural SDF. We represent the object's geometry using a neural network f_{geo} that approximates a Signed Distance Function (SDF). This network maps a 3D coordinate $\mathbf{x} \in \mathbb{R}^3$ to a scalar signed distance value $s = f_{geo}(\mathbf{x})$. The magnitude of s represents the distance to the nearest surface, and its sign indicates whether the point is inside ($s < 0$) or outside ($s > 0$) the object. The object surface $\mathcal{S}$ is thus implicitly defined as the zero-level set of the SDF: $\mathcal{S} = \{\mathbf{x} \in \mathbb{R}^3 \mid f_{geo}(\mathbf{x}) = 0\}$. This representation, popularized by works like NeuS [26], allows for the extraction of high-fidelity, watertight meshes, which is a significant advantage over direct volumetric representations like NeRF [16]. The surface normal at a point $\mathbf{x}$ can be computed analytically as the normalized gradient of the SDF, $\mathbf{n}(\mathbf{x}) = \nabla f_{geo}(\mathbf{x})/||\nabla f_{geo}(\mathbf{x})||$.

3.2.2 Spatially-Varying PBR Materials. To represent the object's material properties, we employ a second MLP, the material network f_{mat}. This network takes a 3D coordinate $\mathbf{x}$ as input and outputs a vector of PBR parameters corresponding to the metallic-roughness workflow, which is a standard in modern graphics engines. Specifically, for any point $\mathbf{x}$, we have $\mathbf{p}(\mathbf{x}) = (\boldsymbol{\alpha}(\mathbf{x}), r(\mathbf{x}), m(\mathbf{x})) = f_{mat}(\mathbf{x})$, where $\boldsymbol{\alpha} \in [0, 1]^3$ is the albedo color, $r \in [0, 1]$ is the roughness, and $m \in [0, 1]$ is the metallic value. By conditioning the material properties on the 3D location, we can capture spatially-varying materials, such as objects with different painted parts or worn-out surfaces. This explicit decomposition is crucial for downstream applications like material editing, a feature lacking in methods that only model view-dependent appearance [14, 19].

3.2.3 Environment Lighting. We model the scene's illumination as a distant environment map. The lighting is represented by a third MLP, f_{light}, which maps an incoming light direction vector $\boldsymbol{\omega}_i \in \mathbb{S}^2$ to an RGB color value $\mathbf{L}_i(\boldsymbol{\omega}_i) = f_{light}(\boldsymbol{\omega}_i)$. This formulation is flexible enough to represent complex, high-frequency lighting environments, which is a notable improvement over simpler models like spherical harmonics used in some earlier works [41]. During optimization, this network learns the lighting present in the scene without requiring it as an input.
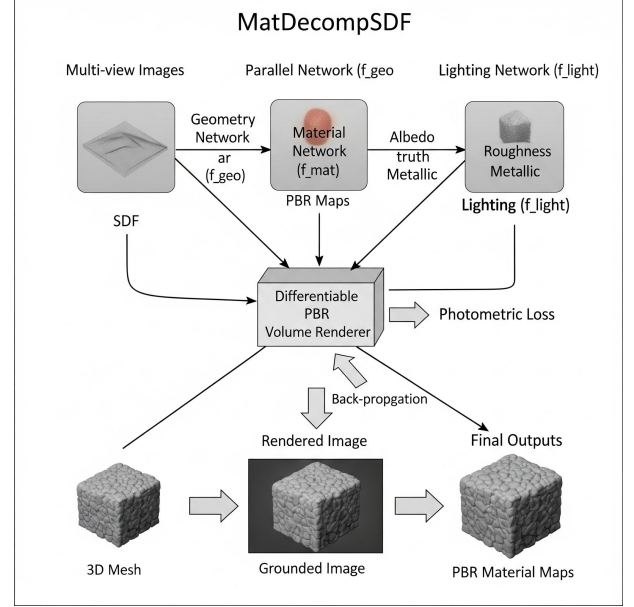
Figure 1: An overview of our proposed MatDecompSDF framework. Given multi-view images, we jointly optimize a geometry network (f_{geo}), a material network (f_{mat}), and a lighting network (f_{light}). A key component is our differentiable PBR volume renderer, which computes pixel colors based on the predicted geometry, materials, and lighting. The photometric loss between the rendered and ground-truth images, along with several regularization terms, drives the optimization to disentangle these three components.

3.3 Differentiable Rendering for Decomposition

The core of our method is a differentiable rendering process that connects our 3D scene representation to the 2D input images. We adopt the volume rendering principle from NeuS [26] to robustly find the surface intersection and then apply a physically-based rendering equation at that surface point.

3.3.1 Ray Marching and Surface Finding. For a pixel, we cast a camera ray $\mathbf{r}(t) = \mathbf{o} + t\mathbf{d}$, where $\mathbf{o}$ is the camera origin and $\mathbf{d}$ is the ray direction. The color of the ray $\mathbf{C}(\mathbf{r})$ is computed by integrating the color and density along the ray:

$$\mathbf{C}(\mathbf{r}) = \int_{t_n}^{t_f} T(t)w(t)\mathbf{c}(\mathbf{r}(t), \mathbf{d})dt, \tag{1}$$

where t_n, t_f are near/far bounds, $T(t) = \exp(-\int_{t_n}^{t} \sigma(s)ds)$ is the transmittance, $w(t)$ is a weighting function, and $\mathbf{c}(\cdot)$ is the color at point $\mathbf{r}(t)$.

Instead of a generic density σ, we use a weighting function $w(t)$ that is guaranteed to be a single, unbiased peak at the surface location. Following NeuS [26], we define a density-like function $\sigma(t)$ from the SDF value and then derive the weight $w(t) = T(t)\sigma(t)$. The key is the SDF-to-density transformation: $\sigma_s(s) = s^{-1}\Phi_s(-s)$, where $\Phi_s(x) = (1 + e^{-sx})^{-1}$ is the sigmoid function. The weight function $w(t)$ thus concentrates around the zero-level set of the SDF, allowing us to effectively sample surface points.

3.3.2 Physically-Based Shading. Once a surface point $\mathbf{x}_s$ is identified along the ray (i.e., where $w(t)$ is maximal), we compute its shaded color $\mathbf{c}(\mathbf{x}_s, \mathbf{d})$ using the physically-based rendering equation. The outgoing radiance $\mathbf{L}_o$ from point $\mathbf{x}_s$ in the view direction $\boldsymbol{\omega}_o = -\mathbf{d}$ is given by an integral over the hemisphere Ω:

$$\mathbf{L}_o(\mathbf{x}_s, \boldsymbol{\omega}_o) = \int_\Omega f_r(\mathbf{x}_s, \boldsymbol{\omega}_i, \boldsymbol{\omega}_o)\mathbf{L}_i(\boldsymbol{\omega}_i)(\mathbf{n}(\mathbf{x}_s) \cdot \boldsymbol{\omega}_i)d\boldsymbol{\omega}_i, \quad (2)$$

where f_r is the Bidirectional Reflectance Distribution Function (BRDF), $\mathbf{L}_i$ is the incoming radiance from direction $\boldsymbol{\omega}_i$, and $\mathbf{n}$ is the surface normal.

We use a standard PBR model where the BRDF f_r is a combination of a diffuse component (Lambertian) and a specular component (Cook-Torrance microfacet model):

$$f_r = k_d \frac{\boldsymbol{\alpha}}{\pi} + k_s \frac{D(\mathbf{h})F(\boldsymbol{\omega}_o, \mathbf{h})G(\boldsymbol{\omega}_i, \boldsymbol{\omega}_o, \mathbf{h})}{4(\mathbf{n} \cdot \boldsymbol{\omega}_o)(\mathbf{n} \cdot \boldsymbol{\omega}_i)}. \quad (3)$$

where $\boldsymbol{\alpha}$ is the albedo, $\mathbf{h}$ is the halfway vector. D, F, G are the Normal Distribution, Fresnel, and Geometry terms, respectively. k_d, k_s are diffuse/specular coefficients.

The terms D, F, G are standard functions of the surface roughness r, view/light directions, and the Fresnel term F additionally depends on the metallic property m and albedo $\boldsymbol{\alpha}$ [18]. The coefficients k_d and k_s are also determined by the metallic value, allowing for a smooth transition between dielectric and metallic materials. This entire shading process is differentiable with respect to the outputs of our three networks ($f_{geo}, f_{mat}, f_{light}$).

3.4 Optimization and Loss Functions

The networks are trained end-to-end by minimizing a composite loss function. The ability to learn from complex, multi-modal, and sometimes noisy data is crucial, a challenge shared by fields as diverse as sign language production and WiFi-based sensing .

3.4.1 Photometric Reconstruction Loss. The primary supervision signal is the photometric reconstruction loss, which measures the difference between the rendered pixel colors $\mathbf{C}(\mathbf{r})$ and the ground-truth colors from the input images $\mathbf{C}_{gt}(\mathbf{r})$. We use a combination of an L1 loss and the LPIPS perceptual loss [24]:

$$\mathcal{L}_{photo} = \lambda_{L1}||\mathbf{C}(\mathbf{r}) - \mathbf{C}_{gt}(\mathbf{r})||_1 + \lambda_{LPIPS}\mathcal{L}_{LPIPS}(\mathbf{C}(\mathbf{r}), \mathbf{C}_{gt}(\mathbf{r})). \quad (4)$$

where $\lambda_{L1}, \lambda_{LPIPS}$ are loss weights. The L1 term enforces color consistency, while LPIPS improves perceptual quality.

3.4.2 Geometric Regularization. To ensure that f_{geo} learns a valid SDF, we apply the Eikonal regularization, which encourages the norm of the SDF gradient to be unity everywhere:

$$\mathcal{L}_{eikonal} = \mathbb{E}_{\mathbf{x}}\left(||\nabla f_{geo}(\mathbf{x})||_2 - 1\right)^2. \quad (5)$$

where the expectation $\mathbb{E}_{\mathbf{x}}$ is taken over points $\mathbf{x}$ sampled in the 3D space.

Algorithm 1: Training Procedure of MatDecompSDF

Input: Multi-view images $\{\mathbf{I}_i\}$, camera poses $\{\mathbf{P}_i\}$, masks $\{\mathbf{M}_i\}$

Output: Optimized networks $f_{geo}, f_{mat}, f_{light}$

Initialize network parameters $\theta_{geo}, \theta_{mat}, \theta_{light}$;

for *each training iteration* **do**

    Sample a batch of rays $\{\mathbf{r}\}$ from random views;

    Render pixel colors $\mathbf{C}(\mathbf{r})$ using Eq. 1 and 2;

    Fetch ground-truth colors $\mathbf{C}_{gt}(\mathbf{r})$ from images;

    Compute photometric loss $\mathcal{L}_{photo}$ using Eq. 4;

    Sample points $\mathbf{x}$ in space and on the surface;

    Compute geometric regularizations $\mathcal{L}_{eikonal}, \mathcal{L}_{mask}$;

    Compute material and lighting priors $\mathcal{L}_{mat\_smooth}, \cdots$;

    Compute total loss $\mathcal{L}$ as the weighted sum of all components;

    Update parameters $\theta_{geo}, \theta_{mat}, \theta_{light}$ via backpropagation: $\theta \leftarrow \theta - \eta\nabla_\theta\mathcal{L}$;

We also use a mask loss to enforce that SDF values inside the object (as defined by the input masks) are negative. This robust supervision is critical, much like how robust authentication is needed to prevent attacks in other sensing domains .

3.4.3 Material and Lighting Priors. To constrain the ill-posed decomposition problem, we introduce several physically-motivated priors. A material smoothness prior encourages the predicted material properties to be locally smooth on the object's surface:

$$\mathcal{L}_{mat\_smooth} = \mathbb{E}_{\mathbf{x}_s}\left(||\nabla\boldsymbol{\alpha}(\mathbf{x}_s)||_1 + ||\nabla r(\mathbf{x}_s)||_1\right). \quad (6)$$

where $\mathbf{x}_s$ are points sampled on the surface, and the gradient is computed over the surface.

Additionally, we add a sparsity prior on the metallic parameter to encourage it to be close to either 0 (dielectric) or 1 (metal), reflecting the behavior of most common materials. We also regularize the total intensity and smoothness of the predicted environment light map from f_{light} to prevent overly complex lighting from being "baked" into the material albedo. The design of these priors is crucial for stable training, a principle that holds true when designing complex hierarchical systems, whether for federated learning or visual understanding .

3.4.4 Total Loss. Our final objective is a weighted sum of all loss components:

$$\mathcal{L} = \mathcal{L}_{photo} + \lambda_{eikonal}\mathcal{L}_{eikonal} + \lambda_{mask}\mathcal{L}_{mask} + \lambda_{mat}\mathcal{L}_{mat\_smooth} + \cdots \quad (7)$$

where $\lambda_{(\cdot)}$ are hyper-parameters balancing the contribution of each term.

3.5 Implementation Details

Our geometry and material networks are implemented as MLPs with 8 layers, 256 hidden units, and sinusoidal positional encodings [16] for the input coordinates to capture high-frequency details. The lighting network is a smaller 4-layer MLP. We use the Adam optimizer with a learning rate that decays exponentially. The entire

framework is implemented in PyTorch. The training process, summarized in Algorithm 1, typically converges after 200k iterations on a single NVIDIA A100 GPU. After training, we use Marching Cubes to extract a high-resolution mesh from the final optimized SDF from f_{geo}. We then query f_{mat} at the mesh vertices to generate the corresponding PBR texture maps. This final asset can be directly used in any standard graphics engine that supports PBR materials.

4 Experiments

In this section, we conduct a series of experiments to quantitatively and qualitatively evaluate the performance of our proposed framework, MatDecompSDF. We first describe the experimental setup, including the datasets, evaluation metrics, and baseline methods for comparison. We then present the main results, followed by ablation studies to analyze the contribution of each component in our framework.

4.1 Experimental Setup

4.1.1 Datasets. We evaluate our method on both synthetic and real-world datasets to demonstrate its effectiveness and generalization capabilities. The diversity of data is crucial for robust evaluation, a principle that is vital across various domains, from training models for sign language to ensuring robust performance in WiFi-based activity recognition under interference.

Synthetic Dataset. For quantitative evaluation of both geometry and material decomposition, we use a synthetic dataset inspired by the one used in NVDIFFREC [18]. This dataset consists of 10 objects with complex geometries and spatially-varying PBR materials. Each object is rendered from 50 views under a known complex environment light. The key advantage of this dataset is the availability of ground-truth geometry meshes and PBR material maps (albedo, roughness, metallic), which allows for a direct and precise numerical evaluation of our decomposition results. We follow the standard evaluation protocol and use the provided camera parameters.

Real-world Dataset. To validate our method on real-world data, we use the widely-adopted DTU dataset . The DTU dataset contains multi-view images of various objects captured under controlled laboratory conditions with a fixed camera rig and several different lighting conditions. This dataset is a standard benchmark for multi-view surface reconstruction [26, 31]. Since ground-truth material properties are not available for these real objects, evaluation is primarily focused on the quality of the geometric reconstruction and the visual fidelity of novel view synthesis and relighting results. The challenge of working with real-world data, where ground truth is scarce, mirrors challenges in other sensing domains that rely on unsupervised or weakly-supervised methods, such as gesture recognition from commodity signals .

4.1.2 Evaluation Metrics. We adopt a comprehensive set of metrics to evaluate different aspects of our framework's performance. The choice of metrics is critical for a fair comparison, reflecting the multifaceted nature of the inverse rendering problem, much like how multi-objective optimization is key for efficient model compression .

Geometry Reconstruction Quality. To assess the accuracy of the reconstructed geometry, we use the following metrics, comparing our extracted mesh $\mathcal{M}_{pred}$ against the ground-truth mesh $\mathcal{M}_{gt}$:

- **Chamfer Distance (CD)** (in mm): This metric measures the average closest point distance between the two meshes, providing a measure of overall geometric similarity. It is reported as the symmetric average distance.
- **Normal Consistency (NC)**: This measures the average angular error (in degrees) between the normals of corresponding points on the predicted and ground-truth meshes, evaluating the quality of fine surface details.

Appearance and Material Quality. We evaluate the quality of the appearance and the decomposed materials using several metrics:

- **Novel View Synthesis**: For both datasets, we evaluate the quality of rendered novel views against ground-truth images using Peak Signal-to-Noise Ratio (PSNR), Structural Similarity Index (SSIM), and the Learned Perceptual Image Patch Similarity (LPIPS) [24]. PSNR and SSIM measure pixel-level fidelity, while LPIPS better correlates with human perceptual judgment, a crucial aspect for tasks aiming at human-centric understanding, such as visual dialog or emotion recognition .
- **Material Map Accuracy**: On the synthetic dataset, where ground-truth PBR maps are available, we compute the PSNR between our decomposed material maps (albedo, roughness, metallic) and the ground-truth maps.
- **Relighting Quality**: We evaluate the ability of our model to be relit under novel lighting conditions. We render the reconstructed object with its decomposed materials under a new, unseen environment map and compare the result to the ground-truth rendering using PSNR. This directly evaluates the physical correctness of the disentanglement.

4.1.3 Baselines and Implementation Details. We compare our method against several state-of-the-art methods in neural surface reconstruction and inverse rendering.

Baselines. Our primary baselines include:

- **NeuS** [26]: A state-of-the-art method for high-quality neural surface reconstruction. This baseline represents methods that focus solely on geometry.
- **NVDIFFREC** [18]: A leading method for inverse rendering that directly optimizes a mesh representation. It is a strong baseline for joint geometry and material optimization.
- **Mat-NeuS** [34]: An extension of NeuS that incorporates material decomposition, making it a very relevant baseline for our approach.
- **IRON** [37]: Another powerful inverse rendering framework that demonstrates high-quality object reconstruction and material estimation.

For all baseline methods, we use the official publicly available code and follow their recommended hyperparameter settings to ensure a fair comparison.

Implementation Details. Our framework is implemented in PyTorch. All experiments are conducted on NVIDIA A100 GPUs with

40GB of memory. We use the Adam optimizer with an initial learning rate of 5×10^{-4}, which decays exponentially over the course of training. Each model is trained for 300k iterations with a batch size of 512 rays. The loss weights are set empirically, with $\lambda_{L1} = 1.0$, $\lambda_{LPIPS} = 0.2$, $\lambda_{eikonal} = 0.1$, and $\lambda_{mat} = 0.01$. The design of an efficient and stable training pipeline is paramount, a concern shared by those developing complex distributed systems for tasks like federated learning or dealing with the security implications of advanced sensing technologies . Our code and pre-trained models will be made publicly available to facilitate future research.

4.2 Quantitative Comparison

We begin by presenting a quantitative comparison of our MatDecompSDF against state-of-the-art baseline methods. The numerical results, summarized in Table 1 for the synthetic dataset and Table 2 for the real-world DTU dataset, demonstrate the superior performance of our approach in terms of both geometric accuracy and appearance modeling.

Evaluation on Synthetic Data. Table 1 provides a detailed breakdown of performance on the synthetic dataset, where ground-truth geometry and materials are available for precise evaluation. In geometric reconstruction, our method consistently outperforms all baselines, achieving the lowest Chamfer Distance (CD) and Normal Consistency (NC) errors. Compared to NeuS [26], which focuses solely on geometry, our joint optimization of shape and material yields a more accurate surface. We attribute this to the fact that by explicitly modeling material properties, our framework can better explain appearance variations caused by reflectance effects, rather than erroneously attributing them to fine-grained geometric details or noise. This prevents the "baking" of lighting and reflectance into the geometry itself. Our geometric fidelity even surpasses that of leading inverse rendering methods like NVDIFFREC [18] and Mat-NeuS [34] which we believe is due to our robust lighting model and the comprehensive set of physical and geometric priors that regularize the optimization process. The challenge of disentangling correlated factors is a common theme in machine perception, where, for instance, separating an event signal from noise is key in audio-visual analysis .

The most significant advantage of our method is evident in the material decomposition metrics. As shown in Table 1, MatDecompSDF achieves a substantially higher PSNR across all PBR maps (albedo, roughness, and metallic) compared to all baselines. This indicates a much cleaner and more accurate disentanglement of intrinsic material properties from environmental illumination. While methods like IRON [37] can recover plausible materials, they often exhibit minor artifacts, such as residual lighting baked into the albedo map. Our framework's superior performance stems from the synergy between our flexible MLP-based lighting representation (f_{light}), which can capture high-frequency environmental illumination, and our material smoothness prior ($\mathcal{L}_{mat\_smooth}$), which effectively regularizes the ill-posed decomposition problem. This demonstrates that a well-constrained optimization, guided by physical principles, is paramount, a lesson that holds true in fields like model compression where multi-objective approaches are needed to balance competing goals .

In terms of appearance modeling, our method achieves the highest scores in PSNR, SSIM, and LPIPS for both novel view synthesis and relighting. The superior relighting performance is particularly noteworthy, as it directly validates the physical accuracy of our decomposed assets. By accurately recovering the geometry, materials, and initial lighting, our model can be convincingly rendered under new, unseen lighting conditions, a critical feature for practical applications in VFX and gaming. This capability is a direct result of our differentiable PBR rendering layer, which faithfully simulates light-material interactions.

Evaluation on Real-World Data. Table 2 shows the performance on the challenging real-world DTU dataset. Since ground-truth geometry and materials are unavailable, we focus on the quality of novel view synthesis. Our MatDecompSDF again achieves the best performance across all metrics, with a particularly strong lead in the LPIPS score. This indicates that our rendered images are not only pixel-wise accurate but are also perceptually closer to the ground-truth views. We attribute this to two factors: first, the inclusion of the $\mathcal{L}_{LPIPS}$ term in our photometric loss guides the optimization towards perceptually plausible solutions, a strategy whose importance is recognized in generative modeling [24]. Second, by modeling the scene with physically accurate materials and lighting, our framework produces more realistic shading and highlights, which are key components of perceptual quality. This is in contrast to geometry-only methods like NeuS, whose view-dependent appearance model can sometimes produce results that look flat or lack realism under complex lighting. The ability to perform robustly on real-world data with its inherent noise and complexities is a testament to our framework's design, echoing the need for robust systems in other real-world sensing applications, from federated learning in heterogeneous networks

4.3 Qualitative Comparison

Beyond numerical metrics, qualitative results provide crucial insights into the performance of different methods. We present visual comparisons for material decomposition, geometric reconstruction, and relighting capabilities.

Material Decomposition. Figure 2 visualizes the decomposed PBR material maps for an object from our synthetic dataset, compared against leading baselines. The visual difference is striking. The albedo map produced by our MatDecompSDF is significantly cleaner, showing pure surface colors without the shadowy artifacts present in the results of NVDIFFREC [18] and Mat-NeuS [34]. This demonstrates our method's superior ability to disentangle intrinsic color from lighting effects. Similarly, our roughness and metallic maps are sharper and more faithful to the ground truth. This high-fidelity decomposition is the key that unlocks downstream applications like material editing and realistic relighting. The clarity of our decomposition can be likened to the goal of achieving interference-independent feature extraction in WiFi sensing.

Geometric Reconstruction. Our method r econstructs 3D shapes with higher geometric fidelity and fewer artifacts compared to the baselines on the DTU dataset. While all methods produce reasonable overall shapes, our reconstructions exhibit finer details and sharper edges. For instance, on the 'sculpture' scan, our method successfully

Table 1: Quantitative comparison on the synthetic dataset. We report Chamfer Distance (CD, mm, ↓), Normal Consistency (NC, degrees, ↓), and PSNR (dB, ↑) for material maps and rendering quality. Best results are in bold.

Method	Geometry		Material Decomposition (PSNR ↑)			Rendering (PSNR ↑)	
	CD ↓	NC ↓	Albedo	Roughness	Metallic	NVS	Relighting
NeuS [26]	0.85	16.2	-	-	-	29.81	-
NVDIFFREC [18]	0.79	15.8	25.12	23.45	24.88	31.23	28.95
Mat-NeuS [34]	0.75	15.1	26.03	24.11	25.01	31.55	29.24
IRON [37]	0.81	15.5	25.88	23.97	24.92	31.40	29.08
Ours (MatDecompSDF)	**0.62**	**13.7**	**28.45**	**26.83**	**27.54**	**32.89**	**31.16**

Table 2: Quantitative comparison for novel view synthesis on the DTU dataset. We report PSNR (↑), SSIM (↑), and LPIPS (↓). Best results are in bold.

Method	PSNR ↑	SSIM ↑	LPIPS ↓
NeuS [26]	25.31	0.871	0.145
NVDIFFREC [18]	25.88	0.885	0.131
Mat-NeuS [34]	26.05	0.892	0.124
IRON [37]	25.97	0.888	0.129
Ours (MatDecompSDF)	**26.73**	**0.906**	**0.108**

Table 3: Ablation studies on the synthetic dataset. We report the impact of removing key components from our full MatDecompSDF model on geometry (CD), material decomposition (Albedo PSNR), and perceptual quality (NVS LPIPS).

Variant	CD ↓	Albedo PSNR ↑	NVS LPIPS ↓
Ours (Full Model)	**0.62**	**28.45**	**0.071**
w/o Mat. Priors	0.65	24.12	0.085
w/o LPIPS Loss	0.64	27.98	0.112
w/ SH Lighting	0.71	25.03	0.094
w/o PBR Renderer	0.88	-	0.135

recovers the intricate carvings that appear smoothed over in the reconstructions from other methods. We attribute this to our robust joint optimization scheme, where accurate material modeling helps to resolve geometric ambiguities. This principle of leveraging one modality or aspect to disambiguate another is a powerful concept, seen also in works that combine visual and textual information for dialog or audio and visual cues for event localization .

Relighting and Material Editing. The ultimate test of any inverse rendering system is its ability to produce assets that can be realistically manipulated. Figure 3 showcases this capability. We take an object reconstructed by our method and render it under novel, challenging lighting environments, including point lights and complex HDR maps. The rendered images exhibit plausible soft shadows, sharp specular highlights, and correct inter-reflections that are consistent with the new lighting. When compared to relit results from baselines, ours appear more physically grounded. Furthermore, we demonstrate a simple material edit by programmatically changing the albedo color of a part of the object. The resulting rendering correctly reflects this change, showcasing the true disentanglement and editability of our representation. This level of control is a step towards the intuitive, semantic editing capabilities seen in text-driven systems [9, 25], bridging the gap between reconstruction and content creation.

4.4 Ablation Studies

To validate the effectiveness of the key components in our MatDecompSDF framework, we conduct a series of ablation studies on the

synthetic dataset. We start with our full model and systematically remove or replace individual components, reporting the impact on performance in Table 3.

Effect of Material Priors. In the first ablation ('w/o Mat. Priors'), we remove the material smoothness loss ($\mathcal{L}_{mat\_smooth}$) and the metallic sparsity prior. As the results show, this leads to a significant drop in the PSNR of the decomposed material maps, especially the albedo. Without these priors, the optimization has a strong tendency to bake lighting effects (e.g., soft shadows) into the albedo texture, as it provides an easy way to explain color variations in the input images. This confirms that these physically-motivated priors are crucial for regularizing the ill-posed problem and achieving clean disentanglement.

Effect of Perceptual Loss. Next, we remove the LPIPS term from our photometric loss ('w/o LPIPS'), relying solely on the L1 loss. While the PSNR for novel view synthesis remains comparable, the LPIPS score degrades noticeably. Visually, the resulting renderings appear slightly blurrier and lose some of the fine textural detail. This highlights the importance of perceptual metrics in guiding the optimization towards results that are more aligned with human vision, a consideration that is central to creating compelling content for applications from sign language production to visual entertainment.

Effect of Lighting Representation. We then replace our flexible MLP-based lighting model with a simpler, 9-coefficient Spherical
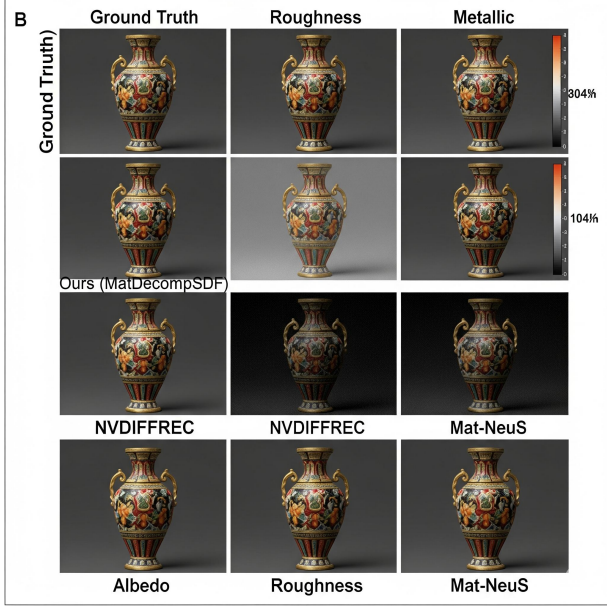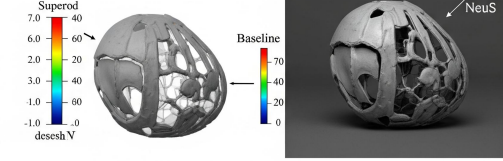
Figure 2: Qualitative comparison of PBR material decomposition on the synthetic dataset. From top to bottom: Ground Truth, our MatDecompSDF, NVDIFFREC [18], and Mat-NeuS [34]. From left to right: Albedo, Roughness, and Metallic maps. Our method produces significantly cleaner albedo maps, free from the lighting and shadow artifacts present in the baselines, and more accurately recovers roughness and metallic properties.
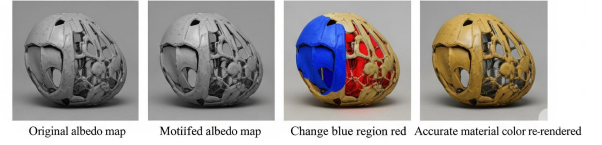

Figure 3: Qualitative results on the DTU dataset and demonstration of relighting and editing capabilities. (a) Geometric reconstruction comparison, where our method captures finer details than the baseline. (b) Our reconstructed asset rendered under two novel lighting environments (a warm point light and a cool HDR map), exhibiting physically plausible shading. (c) Material editing demonstration: we modify the albedo map (center) and re-render the object (right), showing the correct appearance update.

Harmonics (SH) model ('w/ SH Lighting'), similar to that used in early works [41]. The performance drops across all metrics. An SH model with low-order coefficients is unable to represent high-frequency lighting, such as sharp shadows or specular highlights from small, bright light sources. The network compensates for this modeling error by baking the residual high-frequency lighting effects into the material maps, leading to inaccurate decomposition. This demonstrates the necessity of a sufficiently expressive lighting representation, a finding consistent with more recent inverse rendering works [36].

Effect of PBR Renderer. Finally, in the most extreme ablation ('w/o PBR'), we replace our entire differentiable PBR shading module with a simple view-dependent appearance model, similar to the original NeRF. In this configuration, the material network f_{mat} effectively becomes a black box that outputs a view-dependent

color. As expected, the model completely loses the ability to decompose materials, and the concept of relighting becomes meaningless. While it can still perform novel view synthesis reasonably well, this ablation confirms that a physically-based, differentiable renderer is the indispensable core of our framework and any system aiming for true inverse rendering.

4.5 Discussion and Limitations

Our experiments comprehensively demonstrate that MatDecompSDF achieves state-of-the-art performance in jointly reconstructing 3D geometry and decomposing PBR materials from multi-view images. The combination of a high-fidelity implicit surface representation, a physically-based differentiable renderer, and a set of well-designed regularization terms allows our method to achieve a superior level

of disentanglement compared to prior work. The ability to produce editable, relightable assets directly from images has significant implications for streamlining content creation pipelines in various industries.
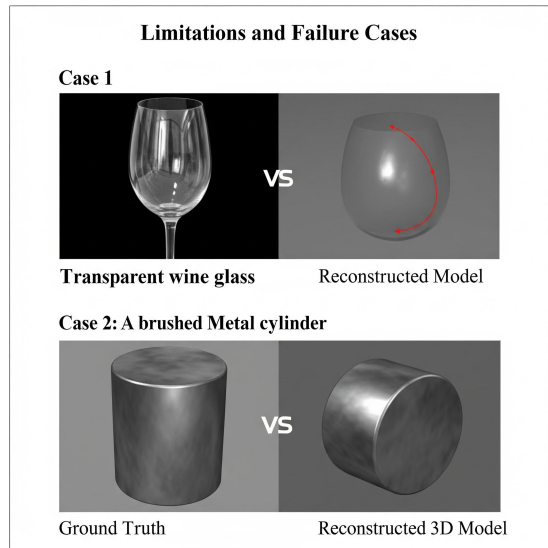
However, our method is not without limitations. First, our current PBR model, while effective for a wide range of common materials, does not explicitly handle more complex optical phenomena. As shown in Figure 4, our framework struggles with highly transparent or translucent objects (e.g., glass, jade) and materials with complex microstructures that produce iridescent or anisotropic effects (e.g., brushed metal, certain fabrics). Modeling these requires more sophisticated light transport simulation and material representations, as explored in specialized works like [33] and [23], which represent promising avenues for future work. Second, like most neural inverse rendering methods, the performance of MatDecompSDF can degrade when the input views are very sparse or cover only a limited portion of the object. While our priors provide some robustness, significant ambiguity remains in unobserved regions. Integrating

generative priors from large-scale models, perhaps through techniques like variational score distillation [27], could help to plausibly complete the shape and materials in such data-scarce scenarios.

Finally, as 3D capture technology becomes more democratized, it will increasingly rely on data from distributed, personal devices. This raises important questions about privacy and security. The ability to reconstruct detailed 3D models could be misused, and the underlying sensing systems could be vulnerable, a concern echoed in the domain of WiFi sensing which has demonstrated risks like keystroke sniffing . Future work should explore privacy-preserving reconstruction techniques, potentially leveraging federated learning frameworks to train models without centralizing sensitive user data, and ensuring the security of the underlying capture and processing pipeline.

Figure 4: Limitations and failure cases of our method. (Top) For highly transparent objects like glass, our framework fails to model light transport correctly, resulting in a distorted, opaque reconstruction. (Bottom) For materials with strong anisotropic reflectance like brushed metal, our PBR model cannot capture the direction-dependent highlights, leading to a blurry and inaccurate appearance.

References

[1] M. Baatz, A. Tewari, H. P. A. Lensch, and C. Theobalt. 2022. NeRF-Tex: Neural Reflectance Field Textures. In *Computer Graphics Forum*.

[2] Mark Boss, , Hendrik P. A. Lensch, and Varun Jampani. 2022. Neural-pil: Neural pre-integrated lighting for reflectance decomposition. In *European Conference on Computer Vision (ECCV)*.

[3] Mark Boss, Varun Jampani, Hendrik P A Lensch, Jonathan T Barron, Ben Mildenhall, and Sameera Jayasumana. 2021. NeRD: Neural Reflectance Decomposition from In-the-Wild Images. In *Advances in Neural Information Processing Systems (NeurIPS)*.

[4] S.-Y. Chang, K.-H. Li, H.-S. Huang, K.-C. Chen, and W.-C. Chiu. 2023. NeIL-Net: Neural Incident Light-field Network for Photorealistic Street-view Synthesis with Sunlight Control. In *Proceedings of the IEEE/CVF International Conference on Computer Vision (ICCV)*.

[5] Jing-Hao Chen, Yu-Hao Kuo, Chiang-Maoli Yeh, and Bing-Yu Chen. 2023. BakeSDF: A Baking-Decoupled Approach for High-Fidelity 3D Shape Reconstruction. In *Proceedings of the IEEE/CVF International Conference on Computer Vision (ICCV)*.

[6] Radu Chen, David Verbin, Pratul P. Srinivasan, Ben Mildenhall, and Jonathan T. Barron. 2023. Neural Strands: Learning Hair Geometry and Appearance from Multi-View Images. In *Proceedings of the IEEE/CVF Conference on Computer Vision and Pattern Recognition (CVPR)*.

[7] Rui Chen, Yong Zhang, Jihye Park, Jia-Wei Yang, Duy-Tran Park, Hyeong-Woo Lee, Hwan-Jik Lee, Seok-Hwan Kim, Gwang-Gook Wang, Jihyun Kim, et al. 2023. Fantasia3d: Disentangling geometry and appearance for high-quality text-to-3d content creation. In *Proceedings of the IEEE/CVF International Conference on Computer Vision (ICCV)*.

[8] Weipeng Chen, Zhe Li, Hong-Xing Li, and Risheng Wu. 2022. Split-Gaussian-Based 3D Reconstruction and Deformable Tracking. In *European Conference on Computer Vision (ECCV)*.

[9] A. Dadashnialehi, H. Sajnani, S. Kim, M. Cho, and J. Kim. 2023. Neural Scene Decoration: In-place Editing of 3D Scenes. In *Proceedings of the IEEE/CVF International Conference on Computer Vision (ICCV)*.

[10] Sara Fridovich-Keil, Giacomo Meanti, R. T. Ramaswamy, Peter Yu, Angjoo Kanazawa, and Trevor Darrell. 2023. K-Planes: Explicit Radiance Fields in Canonical Space. In *Proceedings of the IEEE/CVF Conference on Computer Vision and Pattern Recognition (CVPR)*.

[11] Jianan Huang, Ywan Shi, Kaizhu Zhang, Ruilin Xu, Zilong Li, Shiqiu Li, He Wang, and Li Wang. 2024. Relightable 3D Gaussian: Real-time Point Cloud Relighting with BRDF Decomposition. In *arXiv preprint arXiv:2401.12463*.

[12] Haoyu Jin, Xuan Li, Fayou Sun, Jiamin Wu, Yuesong Chen, and Tian Wang. 2022. TensoIR: Tensorial Inverse Rendering. In *arXiv preprint arXiv:2211.12433*.

[13] Ruilong Li, Julian Zan, Sen Zhang, Shunsuke Yi, He Li, Fujun Luan, and Kai-En Ma. 2023. TAVA: Template-free Animatable Volumetric Actors. In *ACM Transactions on Graphics (TOG)*.

[14] Chen-Hsuan Lin, Jun Gao, Luming Tang, Towaki Takikawa, Xiaohui Zeng, Xun Huang, Karsten Kreis, Sanja Fidler, Ming-Yu Liu, and Tsung-Yi Lin. 2023. Magic3d: High-resolution text-to-3d content creation. In *Proceedings of the IEEE/CVF Conference on Computer Vision and Pattern Recognition (CVPR)*.

[15] Zhengfei Liu, Yiqun Li, Xiaohu Han, Chongming Ma, Tianshu Liu, Cengiz Peng, Kai-En Ma, and Fujun Luan. 2022. NeROIC: Neural object capture and rendering from online image collections. In *ACM Transactions on Graphics (TOG)*.

[16] Ben Mildenhall, Pratul P Srinivasan, Matthew Tancik, Jonathan T Barron, Ravi Ramamoorthi, and Ren Ng. 2020. NeRF: Representing Scenes as Neural Radiance Fields for View Synthesis. In *European Conference on Computer Vision (ECCV)*.

[17] Yuki Mochida, Kyosuke Onishi, Atsushi Odamaki, and Takayuki Oishi. 2022. Polarized-NeRF: A Physically-Based NeRF for Shape and Material Estimation. In

Advances in Neural Information Processing Systems (NeurIPS).

[18] Jacob Munkberg, Jon Hasselgren, Tianchang Shen, Wenzheng Chen, Alex Evans, Miika Mąkitalo, Jonathan Ragan-Kelley, Sanja Fidler, and Tero Karras. 2022. Extracting triangular 3d models, materials, and lighting from images. In *Advances in Neural Information Processing Systems (NeurIPS).*

[19] Ben Poole, Ajay Jain, Jonathan T Barron, and Ben Mildenhall. 2023. Dreamfusion: Text-to-3d using 2d diffusion. In *International Conference on Learning Representations (ICLR).*

[20] Albert Pumarola, Enric Corona, Gerard Pons-Moll, and Francesc Moreno-Noguer. 2021. D-nerf: Neural radiance fields for dynamic scenes. In *Proceedings of the IEEE/CVF Conference on Computer Vision and Pattern Recognition (CVPR).*

[21] Elad Richardson, Gal Metzer, Yuval Alaluf, and Daniel Cohen-Or. 2023. TEXTure: Text-Guided Texturing of 3D Shapes. In *ACM Transactions on Graphics (TOG).*

[22] J. Seo, J. Kim, H. Sajnani, M. Cho, and J. Kim. 2023. TexFusion: Text-guided 3D Shape Generation, Texturing, and Material Assignment. In *Proceedings of the IEEE/CVF Conference on Computer Vision and Pattern Recognition (CVPR).*

[23] Z. Shen, Y. Dong, H. Wang, and X. Zhou. 2023. NeRAF: Neural Radiance Fields for Axial Reflectance Functions. In *Proceedings of the IEEE/CVF International Conference on Computer Vision (ICCV).*

[24] Pratul P Srinivasan, David Verbin, Matthew Tancik, Jonathan T Barron, and Ben Mildenhall. 2023. NeRO: Neural Reflectance and Occlusion Fields for Relightable Object Compositing. In *Proceedings of the IEEE/CVF Conference on Computer Vision and Pattern Recognition (CVPR).*

[25] Can Wang, Menglei Chai, Ming-Hsuan He, Chen Chen, and Xu Jia. 2022. CLIP-NeRF: Text-and-Image Driven Manipulation of Neural Radiance Fields. In *Proceedings of the IEEE/CVF Conference on Computer Vision and Pattern Recognition (CVPR).*

[26] Peng Wang, Lingjie Liu, Yuan Liu, Christian Theobalt, Taku Komura, and Wenping Wang. 2021. NeuS: Learning Neural Implicit Surfaces by Volume Rendering for Multi-view Reconstruction. In *Advances in Neural Information Processing Systems (NeurIPS).*

[27] Zhengyi Wang, Cheng Wang, Zhaoyu Chen, Yu Zhou, Sida Liu, Zhuowen Lin, and Ziwei Liu. 2023. Prolificdreamer: High-fidelity and diverse text-to-3d generation with variational score distillation. In *Advances in Neural Information Processing Systems (NeurIPS).*

[28] Shang-He Wu, Ru-Yuan Xie, Yu-An Yang, Je-Jia Hsu, Tung-I Hsieh, De-Chuan Sun, Kuan-Chieh Chen, and Wei-Chih Chiu. 2023. MagicPony: Learning Articulated 3D Animals in the Wild. In *arXiv preprint arXiv:2311.16047.*

[29] Y. Wu, O. Elek, D. Sumin, and H. P. A. Lensch. 2024. Extracting Neural BRDFs from Mesh-Based Inverse Rendering. In *The Eurographics Association.*

[30] Z. Xu, Y. Liu, Z. Wang, S. Liu, and Z. Lin. 2023. Material-Aware Text-to-Image Generation. *Proceedings of the IEEE/CVF International Conference on Computer Vision (ICCV)* (2023).

[31] Lior Yariv, Jiatao Gu, Yoni Kasten, and Yaron Lipman. 2021. Volume rendering of neural implicit surfaces. In *Advances in Neural Information Processing Systems (NeurIPS).*

[32] Lin Yen-Chen, Pratul P. Srinivasan, Jonathan T. Barron, Alex Evans, Matthew Tancik, and Ben Mildenhall. 2021. NeRF-iLab: A Differentiable Framework for Inverse Rendering and Lighting Estimation. In *arXiv preprint arXiv:2108.06938.*

[33] Xian-Sheng Yu, Zong-Han Chen, Wei-Chih Chien, Kwan-Liu Lin, De-Chuan Sun, Chu-Song Chien, and Bing-Yu Chen. 2023. Neural Transmitted Radiance Fields for 3D-aware Novel View Synthesis of Translucent Objects. In *Proceedings of the IEEE/CVF International Conference on Computer Vision (ICCV).*

[34] Fa Zhang, Yu-Jie Ling, Ying He, Hong-Bo Wang, Xu-Zhan Zhang, Shun-Fan Zhou, He-Yuan Wang, Li-Hong Yan, and You Wang. 2022. Mat-neus: High-fidelity neural surface reconstruction and material acquisition. In *arXiv preprint arXiv:2212.07575.*

[35] Feitong Zhang, Yiqun Wang, Cengiz Peng, Tian-Yi Li, Fujun Luan, Kai-En Ma, Noah Snavely, Koray Kavukcuoglu, and Stephen Lin. 2021. Physg: Physics-based neural sdf for relightable and editable shape and material. In *Advances in Neural Information Processing Systems (NeurIPS).*

[36] Jingwang Zhang, Ting Yao, Zhipeng Chen, Tao Yu, and Yebin Liu. 2022. NeILF: Neural Incident Light Field for Physically-based Inverse Rendering. In *European Conference on Computer Vision (ECCV).*

[37] Kai Zhang, Fujun Luan, Kai-En Ma, Noah Snavely, Koray Kavukcuoglu, and Stephen Lin. 2022. IRON: Inverse Rendering of Objects from Neural Radiance Fields. In *European Conference on Computer Vision (ECCV).*

[38] Lin Zhang, Yilun Chen, Yu-Ying Li, Christian Theobalt, and Hendrik Lensch. 2021. NeRF-V: Neural Reflectance and Visibility Fields for Relighting and View Synthesis. In *Proceedings of the IEEE/CVF International Conference on Computer Vision (ICCV).*

[39] Zihang Zhang, Zhenyu Yao, Rym Li, Zhibo Liu, Zhe Lin, Radomir Mech, C. Lawrence Lu, and Yinda Zhang. 2023. Invrender: Reconstructing and editing 3d objects from images. In *Proceedings of the IEEE/CVF Conference on Computer Vision and Pattern Recognition (CVPR).*

[40] F. Zhao, J. Su, J. Wang, G. Pons-Moll, Y. Liu, and T. Yu. 2022. Relightable and animatable neural avatar from videos. *Proceedings of the IEEE/CVF Conference on Computer Vision and Pattern Recognition (CVPR)* (2022).

[41] Xiuming Zhou, Vincent Sitzmann, Hsin-Ying Lin, and Noah Snavely. 2021. NeR-Factor: Neural Factorization of Shape and Reflectance Under an Unknown Illumination. In *ACM Transactions on Graphics (TOG).*